energies

MDPI

Article

Extraction of Time-Domain Characteristics and Selection of Effective Features Using Correlation Analysis to Increase the Accuracy of Petroleum Fluid Monitoring Systems

Abdulilah Mohammad Mayet [1], Seyed Mehdi Alizadeh [2], Karina Shamilyevna Nurgalieva [3], Robert Hanus [4], Ehsan Nazemi [5,*] and Igor M. Narozhnyy [6]

[1] Electrical Engineering Department, King Khalid University, Abha 61411, Saudi Arabia; amayet@kku.edu.sa
[2] Petroleum Engineering Department, Australian College of Kuwait, Kuwait City 13015, Kuwait; s.alizadeh@ack.edu.kw
[3] Department of Development and Operation of Oil and Gas Fields, Saint-Petersburg Mining University, 199106 Saint-Petersburg, Russia; khaibullina_k@mail.ru
[4] Faculty of Electrical and Computer Engineering, Rzeszów University of Technology, 35-959 Rzeszów, Poland; rohan@prz.edu.pl
[5] Imec-Vision Laboratory, Department of Physics, University of Antwerp, 2610 Antwerp, Belgium
[6] Department of Commercialization of Intellectual Activity Resultse Center for Technology Transfer of RUDN University, Mining Oil and Gas Department, RUDN University, 117198 Moscow, Russia; narozhnyy-im@rudn.ru
* Correspondence: ehsan.nazemi@uantwerpen.be

Abstract: In the current paper, a novel technique is represented to control the liquid petrochemical and petroleum products passing through a transmitting pipe. A simulation setup, including an X-ray tube, a detector, and a pipe, was conducted by Monte Carlo N Particle-X version (MCNPX) code to examine a two-by-two mixture of four diverse petroleum products (ethylene glycol, crude oil, gasoline, and gasoil) in various volumetric ratios. As the feature extraction system, twelve time characteristics were extracted from the received signal, and the most effective ones were selected using correlation analysis to present reasonable inputs for neural network training. Three Multilayers perceptron (MLP) neural networks were applied to indicate the volume ratio of three kinds of petroleum products, and the volume ratio of the fourth product can be feasibly achieved through the results of the three aforementioned networks. In this study, increasing accuracy was placed on the agenda, and an RMSE < 1.21 indicates this high accuracy. Increasing the accuracy of predicting volume ratio, which is due to the use of appropriate characteristics as the neural network input, is the most important innovation in this study, which is why the proposed system can be used as an efficient method in the oil industry.

Keywords: computational intelligence; monitoring characteristics; oil and petrochemical fluids; feature extraction; radiation

Citation: Mayet, A.M.; Alizadeh, S.M.; Nurgalieva, K.S.; Hanus, R.; Nazemi, E.; Narozhnyy, I.M. Extraction of Time-Domain Characteristics and Selection of Effective Features Using Correlation Analysis to Increase the Accuracy of Petroleum Fluid Monitoring Systems. *Energies* **2022**, *15*, 1986. https://doi.org/10.3390/en15061986

Academic Editors: Dmitriy Aleksandrovich Martyushev and Freddy Humberto Escobar

Received: 10 February 2022
Accepted: 7 March 2022
Published: 9 March 2022

1. Introduction

Poly-pipelines are mostly applied in the petrochemical industry for oil transmission or its derivatives to distribution centers. Using a pipeline to transport diverse petroleum fluids is highly economic; however, some problems such as mixing various petroleum fluids indicate the significance of extending a sustainable, non-invasive technique to control and detect the interference region. Due to the mentioned issue, a number of verifications have been conducted, which are concisely demonstrated. Salgado et al. established a petrochemical product density detection system, including a CS-137 source and a NaI detector [1]. The MCNPX code was utilized in such an examination. Via an artificial neural network, the scholars could predict the density of petroleum products with high accuracy independent of fluid admixture. Likewise, for Monte Carlo code validation, they staged

a laboratory structure using a cesium source, a glass pipe, and a sodium iodide detector. Various volume percentages were simulated for both oil and water fluids. They could determine the volume percentages with 99% accuracy [2]. In other analyses, the authors simulated two-phase [3–5] and three-phase [6–8] at diverse volumetric percentages and flow regimes. It is worth noting that with different neural networks, such as MLP [9,10], RBF [11,12], an adaptive neuro-fuzzy inference system [13], the Jaya algorithm [14], and the GMDH neural network [15], the mentioned parameters were determined. Although the mentioned studies were able to obtain the volume percentages and types of flow regimes, not using the feature extraction techniques from the received signals reduced the accuracy and increased the computational cost in the presented systems. Nowadays, the application of characteristic derivation methods such as time-domain [16,17], frequency domain [18], and time-frequency domain [19] is of high significance for the authors. In all concerned investigations, the authors have provided various characteristics to distinguish the kind of flow regimes and detect the volume percentages. Sattari et al. applied a GMDH neural network to detect the kind of flow regimes and volume percentages [20]. By MCNPX code, these researchers simulated a frame including a CS-137 source, a Pyrex pipe, and a NaI detector. They derived the time domain features of the detected signal and regarded them as neural network inputs. They could classify all flow regimes and predict volume percentages with an RMSE < 1.1.

Currently, due to numerous advantages, using X-ray tubes is of high prominence for authors. The utilization of X-ray tubes as a source has the following benefits rather than the other sources such as radioisotopes. The X-ray tube can adjust the distributed photon energy, while the photon emission energy is stable in radioisotopes. It is highly noted that the radioisotope functions decline over time; however, the X-ray tube does not work this way. The X-ray tube can be turned on and off, which is highly prominent for individual health when dealing with these instruments. They are also more feasible to transport than radioisotopes. In previous research, Roshani et al. presented a fluid controlling system passing over transfer tubes [21]. Although they forecasted the volumetric ratio of petroleum products with significant precision, seemingly one of the issues in this study is the lack of using characteristic derivation methods. More studies have been performed for detecting the volume percentages of two-phase [22,23] and three-phase [24,25] flows by X-ray tubes. As the scholars believe, the characteristic extraction methods enhance the precision of detecting the sort of flow regimes and volume percentages. The simulated structure in this study becomes validated with numerous experiments in our preceding work [11]. The experiments and, therefore, the simulations have been carried out inside the static situation. The actual running situation is dynamic; however, the reference points for schooling the detection device are fixed, and it is able to be taken into consideration as a static situation. These constant points have been used for schooling the detection device so that you can decide the volume ratio in the detection device in an actual situation. In [26], prompt gamma-ray neutron activation evaluation for the quantitative evaluation was taken into consideration for rapid, non-intrusive and online measurements of multiphase oil/gas/seawater flow. In this study, all the simulations have been taken into consideration in a static situation before being utilized in an actual situation. In [27], the feasibility of the usage of detection of transmitted and scattered gamma radiation for characterization of produced water from offshore oil wells has been demonstrated. By the approach of transmitted and scattered gamma rays and calibration measurements, the salinity and sort of salt within the produced water have been determined. All of the simulations have been in a. static situation; however, they were eventually utilized in an actual situation.

Increasing the accuracy of diagnostic systems is one of the most important challenges for researchers in this field. Inspired by former research, in this study, it is attempted to provide a high-accuracy controlling system that recognizes the volume ratio of diverse oil products. This increase in accuracy has been achieved by extracting time characteristics and finding the most appropriate ones using correlation analysis as well as designing a suitable neural network. The recent paper will be proposed as follows. First, the structure of the

simulation will be illustrated in detail. The second section represents the feature extraction technique to derive the received signal features. In the next part, the MLP neural network will be mentioned, and the results, as well as the precision of the designed networks, will be indicated. Finally, the conclusion is proposed in the last section.

2. Simulation System

The simulation setup includes an X-ray tube, a pipe, and a NaI detector (Figure 1) and was conducted through MCNPX code [28]. A normal industrial X-ray tube was applied in this study. The electron source and a tungsten/rubidium target are embedded in X-ray tubes as the cathode and anode, respectively. Likewise, the shields with an output window, as well as a filter against the output window, are utilized. A perfect X-ray tube simulation by MCNPX code is time-demanding, in which an emitted electron from the cathode responds to the anode and generates an X-ray emission. Since the calculation of photons passing MCNPX code is lower than the electron, in this study, a source of photons mounted in an X-ray tube's shield was considered for a cathode–anode collection. TASMIC, a free package proposed by Hernandez et al. [29], was utilized. It is worth noting that numerous investigations have been performed on X-ray spectra generation by both theoretical and MCNP techniques [30,31]. Figure 2 indicates the normalized conducted X-ray spectrum, as well as the characteristics of X-ray peaks in relevance to the tungsten target (Kα1, Kα2, Kβ1, and Kβ2). The previously mentioned photon source was embedded in a cylinder serving as an X-ray tube layer. The circular profile on the X-ray tube acting as the output window is 5 cm. It is highly important to mention that the cylindrical shape commonly constitutes the X-ray tube shields made up of lead or steel to prevent the converse radiation diffusions generated by X-ray. On the shield surface, a section is left open, as the output window, in order to release the congenial generated X-ray photons. To filter low-energy photons in this research, an aluminum filter having a thickness of 2.5 mm was mounted against the output window.

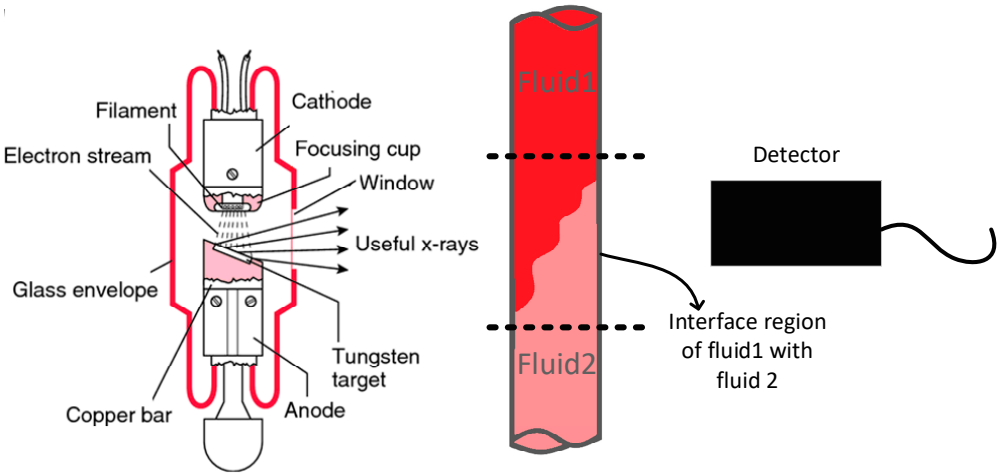

Figure 1. The simulation setup.

Transmitting pipes are applied to transmit different petroleum products, in some sections of which are followed by each other and are combined together. This zone is known as the interface region. In this study, four kinds of petroleum products—ethylene glycol, crude oil, gasoil, and gasoline—with densities of 1.114, 0.975, 0.826, and 0.721 g·cm^{-1}, respectively, are considered as crossing fluids through the pipe. By combining two-by-two of the total of the mentioned products, six admixtures will be achieved. Different volume ratios from 0% to 100% with 5% steps were simulated for six various whole states (in the current study, 118 simulations have been conducted). Data from all the simulations were gathered by an NaI detector using a pulse height tally (tally type F8) in Monte Carlo code and applied for future processing. Pseudo-random number generators (PRNG), which are intensively used in many stochastic algorithms in particle simulations and artificial neural

networks, were used in MCNP code. Furthermore, the "STOP" card was used for obtaining the desired error in simulations.

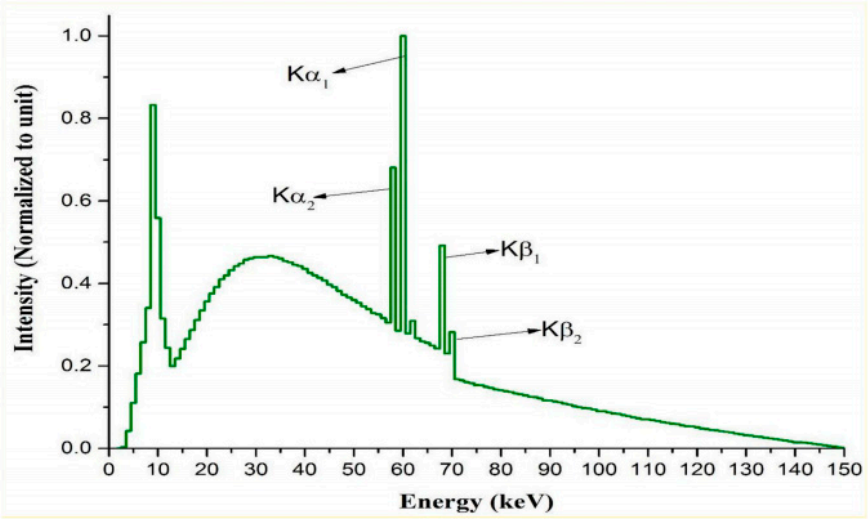

Figure 2. The conducted X-ray spectrum by Monte Carlo simulations via the TASMIC package for 150 kV tube voltage.

3. Feature Extraction

There are various methods for extracting the characteristics of a signal, including the extraction of characteristics in the time domain, in the frequency domain, and combined methods in the time-frequency domain, as well as innovative methods. The purpose of feature extraction is to reduce the size of the signals while preserving the signal properties as well as better interpreting the signals. In this research, the feature extraction technique in the time domain was used. For this purpose, twelve features were extracted from the received signal as follows:

- Average value:

$$m = \frac{1}{N}\sum_{n=1}^{N} x(n) \tag{1}$$

- Standard deviation:

$$STD = \sqrt{\frac{1}{N-1}\sum_{n=1}^{N}|x_n - m|^2} \tag{2}$$

- Fourth-order moment:

$$m_4 = \frac{1}{N}\sum_{n=1}^{N}[x(n) - m]^4 \tag{3}$$

- Root mean square:

$$RMS = \sqrt{m^2 + \sigma^2} \tag{4}$$

- Skewness:

$$g_1 = \frac{m_3}{\sigma^3}, \ m_3 = \frac{1}{N}\sum_{n=1}^{N}[x_n - m]^3 \tag{5}$$

- Kurtosis:

$$g_2 = \frac{m_4}{\sigma^4} \tag{6}$$

- Median:

$$\begin{cases} odd & median = x_k & k = \frac{n+1}{2} \\ even & median = \frac{1}{2}(x_k + x_{k+1}) & k = \frac{n}{2} \end{cases} \tag{7}$$

- Waveform length (WL):

$$\mathrm{WL} = \sum_{n=0}^{N-1}|x_{n+1} - x_n| \tag{8}$$

- Absolute value of the summation of square root (ASS):

$$\mathrm{ASS} = \left|\sum_{n=1}^{N} (x_n)^{0.5}\right| \tag{9}$$

- Mean value of the square root (MSR):

$$\mathrm{MSR} = \frac{1}{N}\sum_{n=1}^{N} (x_n)^{0.5} \tag{10}$$

- Absolute value of the summation of the $^{exp\ \mathrm{th}}$ root (ASM):

$$\mathrm{ASM} = \left|\frac{\sum_{n=1}^{N} (x_n)^{exp}}{N}\right|,\ exp = \begin{cases} 0.05 & if\ (n > 0.25{\cdot}N\ and\ \ n < 0.75{\cdot}N) \\ 0.75 & otherwise \end{cases} \tag{11}$$

- Maximum value:

$$\mathrm{Max} = \mathrm{MAX}\,(x_n) \tag{12}$$

One of the most important challenges of this research is to determine the most effective characteristic for determining the volume ratio of each oil product. Correlation analysis was used for this purpose. The result of the correlation analysis between the extracted characteristics is shown in Figure 3. As shown in this figure, many features are very similar to each other, and their selection as the network input is ineffective. However, the characteristics of the fourth-order moment, skewness, and kurtosis are the least similar to each other, so these characteristics have been selected as the input of the neural network.

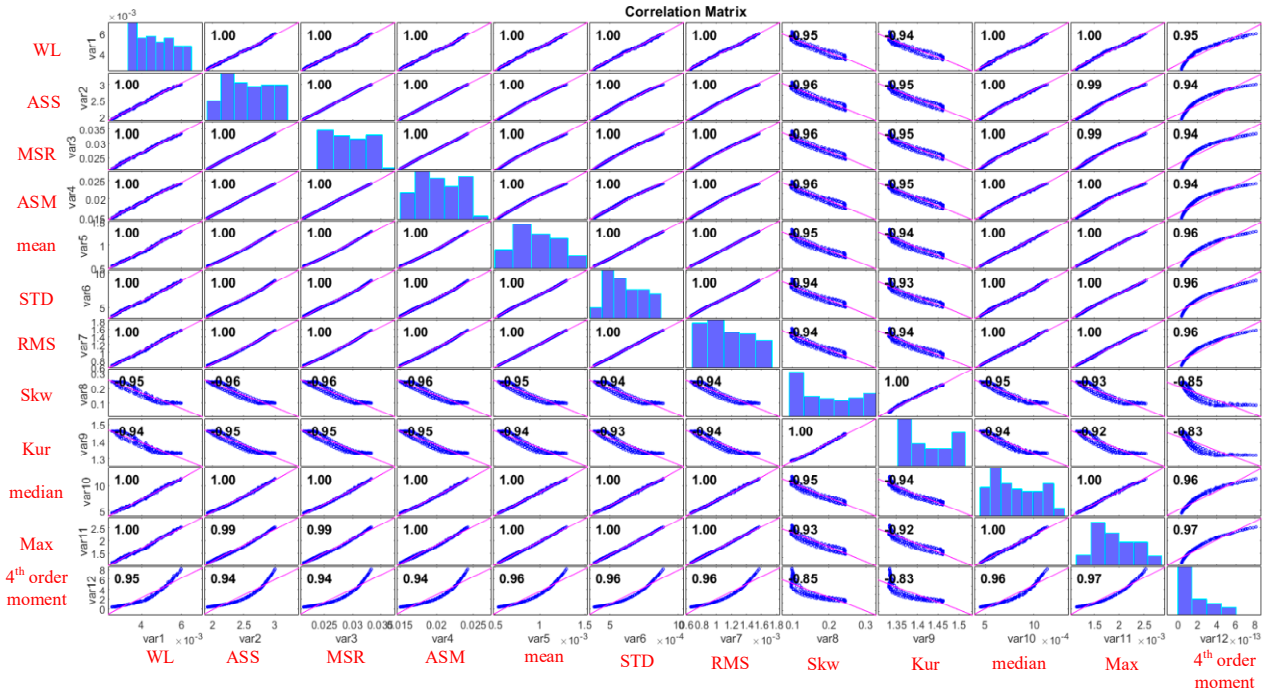

Figure 3. Results of the correlation analysis between all extracted characteristics.

4. Artificial Neural Network

In the past few decades, various advanced computational methods have been applied in various fields of study such as chemical engineering [32–37], electrical and computer engineering [38–41], civil engineering [42–44], mechanical engineering [45–51], petroleum engineering [52–63], and environmental engineering [64,65], etc. The ANN has been demonstrated to be the most potent technique for classification and prediction among the aforementioned computational methods. A type of neural network is based on a

computational unit called a perceptron. A perceptron takes vectors of inputs with real values and calculates a linear combination of these inputs. If the result is more than a threshold value, the perceptron output will be equal to 1 and otherwise equal to −1. Perceptron output is determined by the following equation [66,67]:

$$y = f(\sum_{i=1}^{u} w_i x_i + w_i) \quad (13)$$

In case the perceptron has two inputs x_1 and x_2, it divides the page into two parts, and the equation of the dividing line is determined as follows:

$$w_1 x_1 + w_2 x_2 + w_0 = 0 \quad (14)$$

Therefore, the perceptron can be considered as a hyperplane in the n-dimensional space of the samples. Perceptron sets a value of 1 for samples on one side of the page and −1 for values on the other side of the screen and can only learn examples that are linearly separable. Such examples are cases that can be completely separated by a hyperplane. The purpose of training a perceptron is to find the values of its weights, so that the perceptron generates the correct values for the training examples. Different kinds of numerical calculations [68–78] and soft computing [79–86] have been used in various fields such as electrical engineering problems [87–102], computer sciences problems [103,104], and basic sciences [105–109], etc. In this paper, the perceptron learning algorithm is as follows—this algorithm is shown in Figure 4 as a flowchart:

1. Random values are attributed to weights.
2. Perceptron is applied to each training sample. If the samples are evaluated incorrectly, the values of perceptron weights are corrected.
3. Is all the training properly evaluated?
4. Yes, the end of the algorithm.
5. No, back to step 2.

Networks made of one neuron have limitations. These networks do not have the ability to implement nonlinear functions. Other networks have been suggested to solve this problem. Multilayer perceptron (MLP) networks are among the most useful neural networks. This network is able to perform a nonlinear mapping with high accuracy, and this is what is proposed in engineering problems as the main solution. This network represents feed forward networks, and the output is calculated directly from the input without any feedback. The neuron model in the MLP network includes a nonlinear activation function. The important point to emphasize here is that the activation function must be continuous and derivable at all points. The nonlinearity of the activation function is very important because, otherwise, the network performance will be reduced to the level of the single-layer perceptron.

The obtained data are divided into three categories: training, validation and testing data.

Training dataset: The data that the network sees and learns with. The model fits with these data.

Validation dataset: The dataset that is used as input for the network validating during training to evaluate the training process. The neural network sees these dates but is not trained with them.

Testing dataset: The dataset is injected into the neural network at the end of the training process to test the final performance of the designed network.

The use of the validation test data in the network training process will give us the reassurance to avoid under-fitting and over-fitting problems.

The used validation methods and training processes in this paper are well-known methods in most modeling and optimization problems, which have been used in many studies [110–115]. In several studies [116–125], different mathematical methods such as feature extraction, feature reduction, feature selection, correlation analysis, and numerical calculation, etc., have been used. In this study, feature extraction in the time domain and correlation analysis were used in order to present a novel metering system.

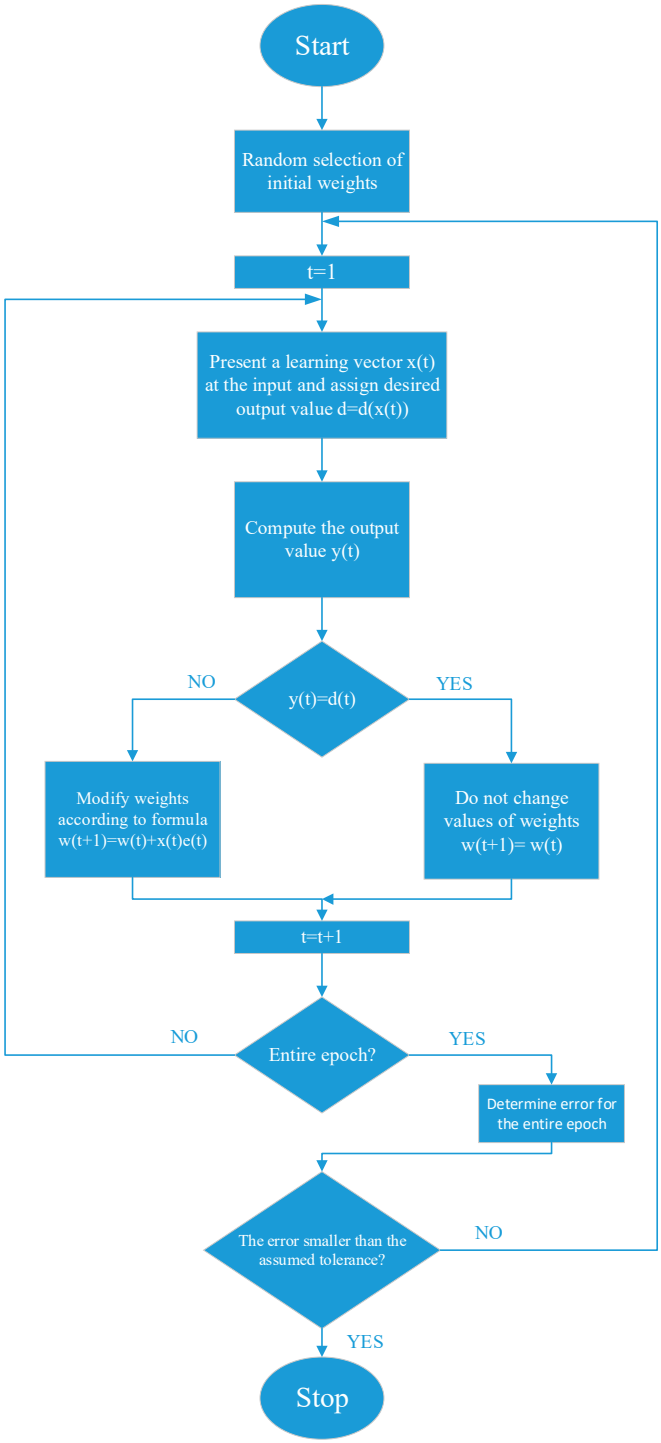

Figure 4. Perceptron learning flowchart.

5. Results Verification

In this study, the characteristics selected using correlation analysis were used as neural network inputs to determine the volume ratio. Three artificial neural networks were established to predict the volume ratios of ethylene glycol, crude oil, and gasoil. The structure of these networks is shown in Figure 5. By recognizing the volume ratio of the three given products, the ratio of the fourth product, i.e., gasoline, can be feasibly estimated. The features of the designed networks are visible in Table 1.

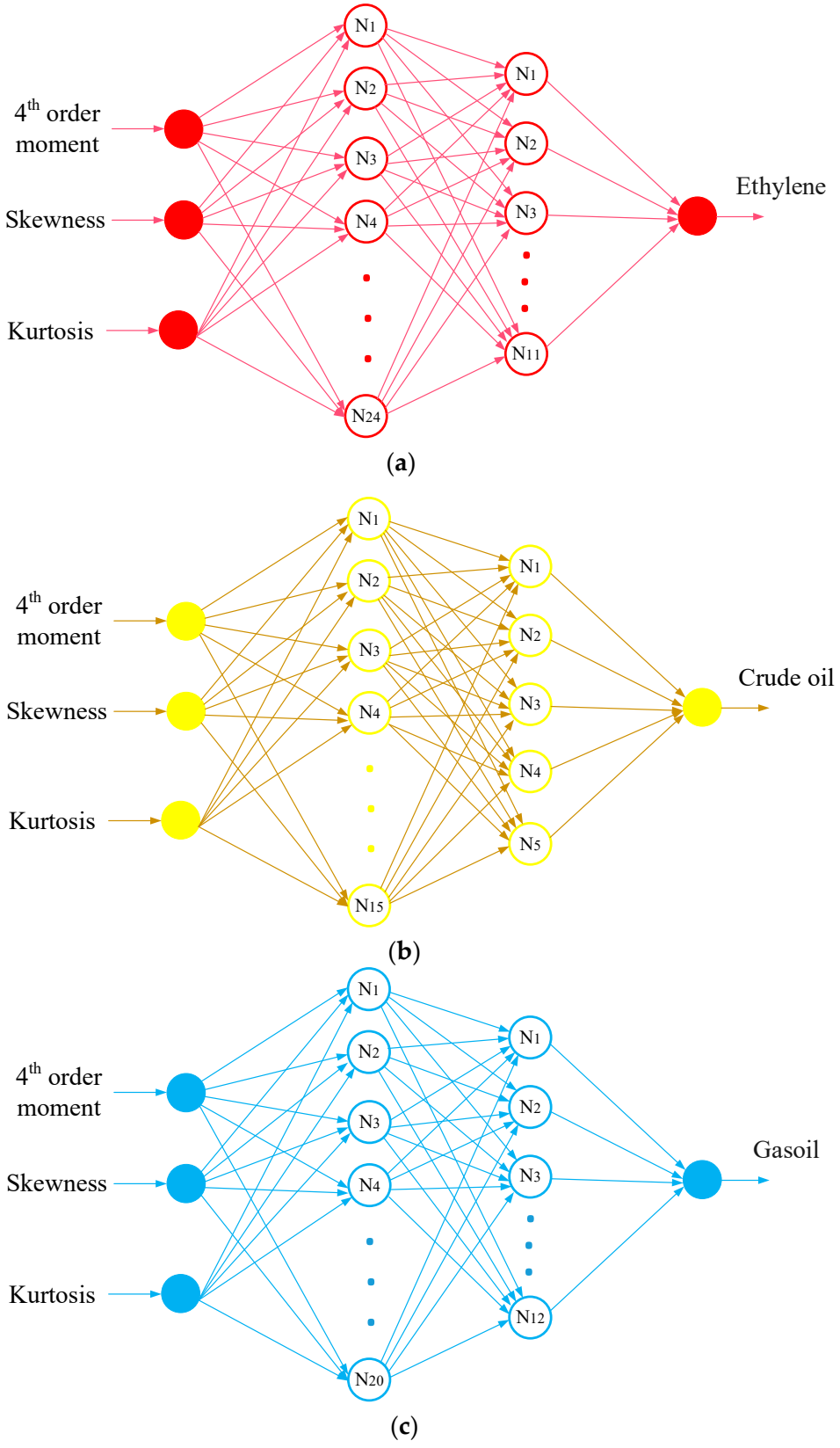

Figure 5. The structure of established MLP neural network for prediction (**a**) ethylene glycol, (**b**) crude oil, and (**c**) gasoil volumetric ratio.

Table 1. The characteristics of designed networks.

ANN Kind	MLP		
	Ethylene Glycol	**Gasoil**	**Crude Oil**
No. of neurons in input layer	3	3	3
No. of neurons in the 1st hidden layer	24	20	15
No. of neurons in the 2nd hidden layer	11	12	5
No. of neurons in the output layer	1	1	1
No. of epoch	500	480	640
Activation function used for each hidden neuron	Tansig	Tansig	Tansig

Regression and error histogram diagrams in relevance to training, validation, and test data are obvious in Figures 6–8 to display the precision of the designated networks. Regarding these three figures, in the regression diagram, the closer the red circles (representing the network output) to the black line (representing the target output), the higher the accuracy of the designed network. The error histogram plot also clearly shows the scatter of error between the desired output and the network output. The most prominent scale for assessing the operation of artificial neural networks is prediction precision. Some of the most significant prediction precision criteria calculated in this study are:

$$\text{Root Mean Square Error (RMSE)} = \frac{\sum_{j=1}^{N} (e_j)^2}{N} \tag{15}$$

$$\text{Mean Absolut Error (MAE)} = \frac{1}{N} \sum_{j=1}^{N} |e| \tag{16}$$

where e is the error, and N presents the data number.

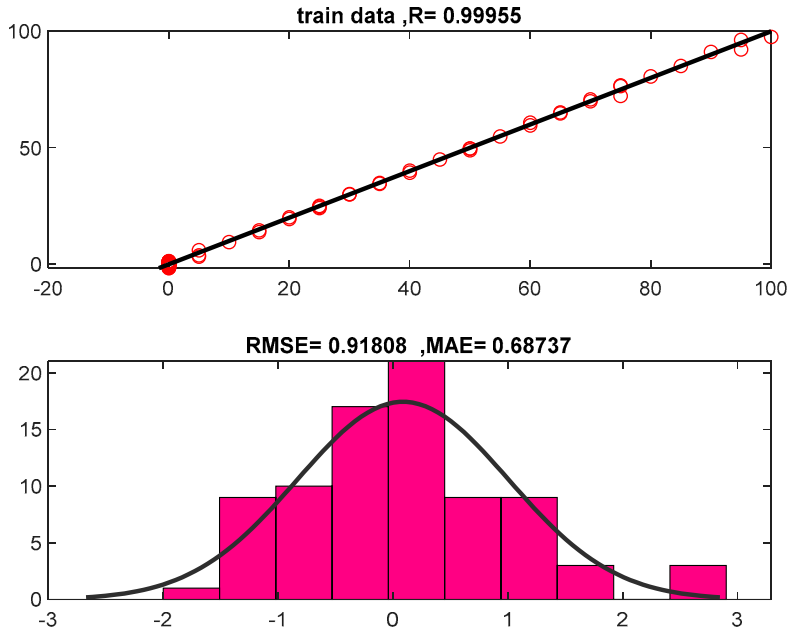

(**a**)

Figure 6. *Cont.*

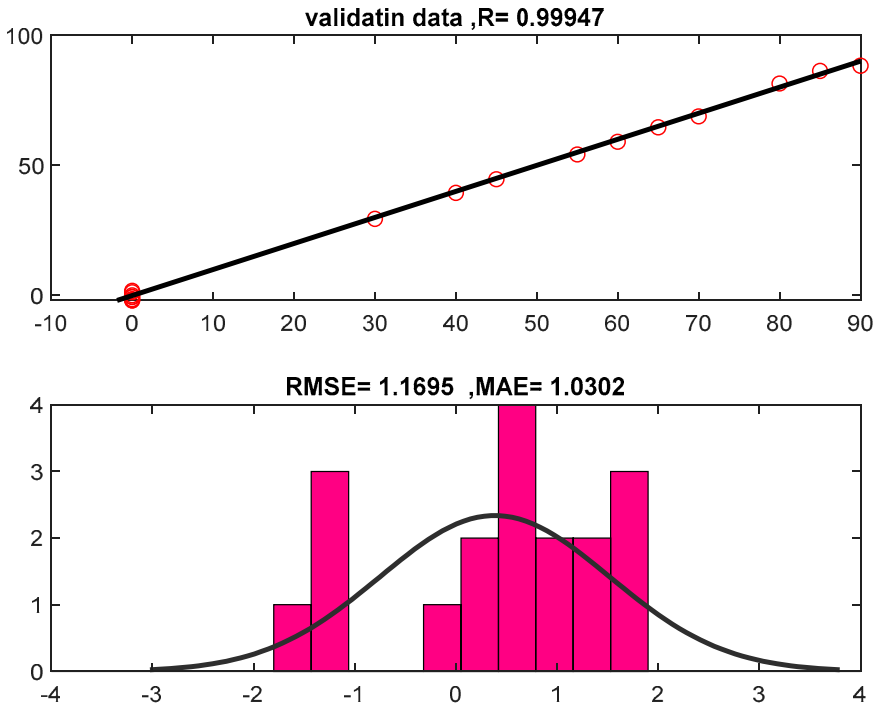

(**b**)

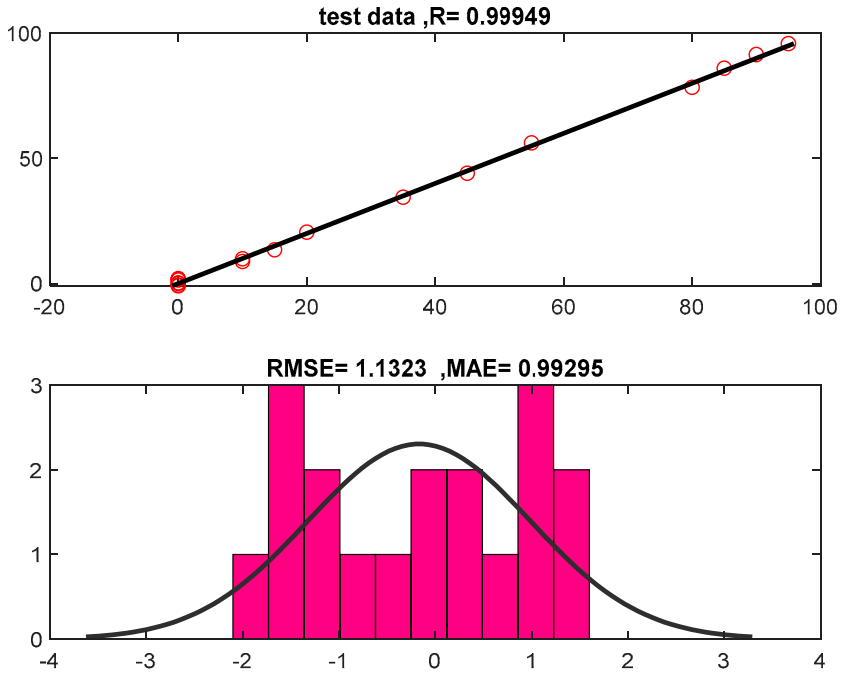

(**c**)

Figure 6. Operation of the designed neural network to recognize the volumetric ratio of ethylene glycol (**a**) train data, (**b**) validation data, and (**c**) test data.

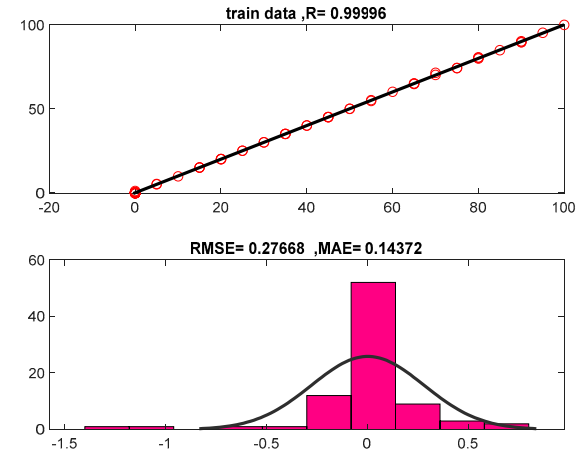

(**a**)

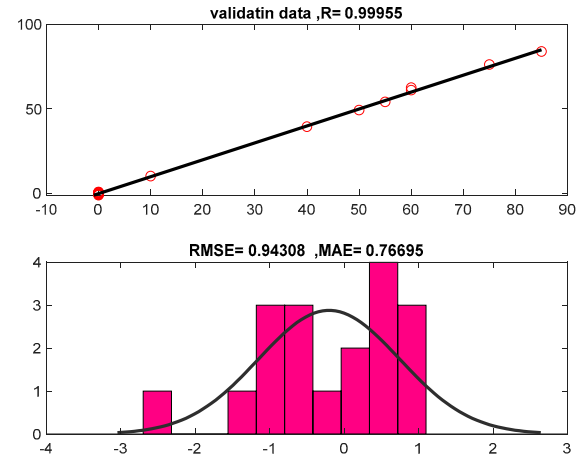

(**b**)

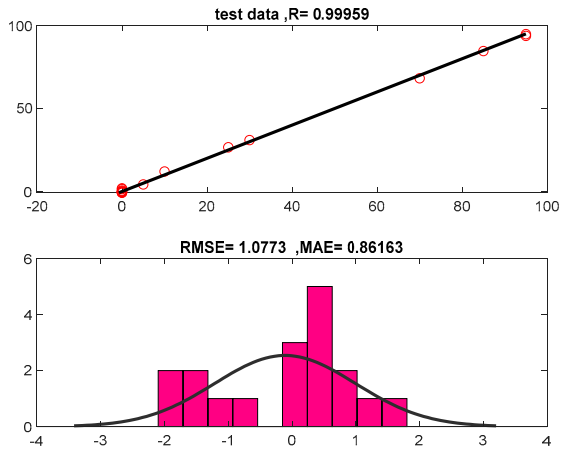

(**c**)

Figure 7. Operation of the designed neural network to detect the volumetric ratio of crude oil (**a**) train data, (**b**) validation data, and (**c**) test data.

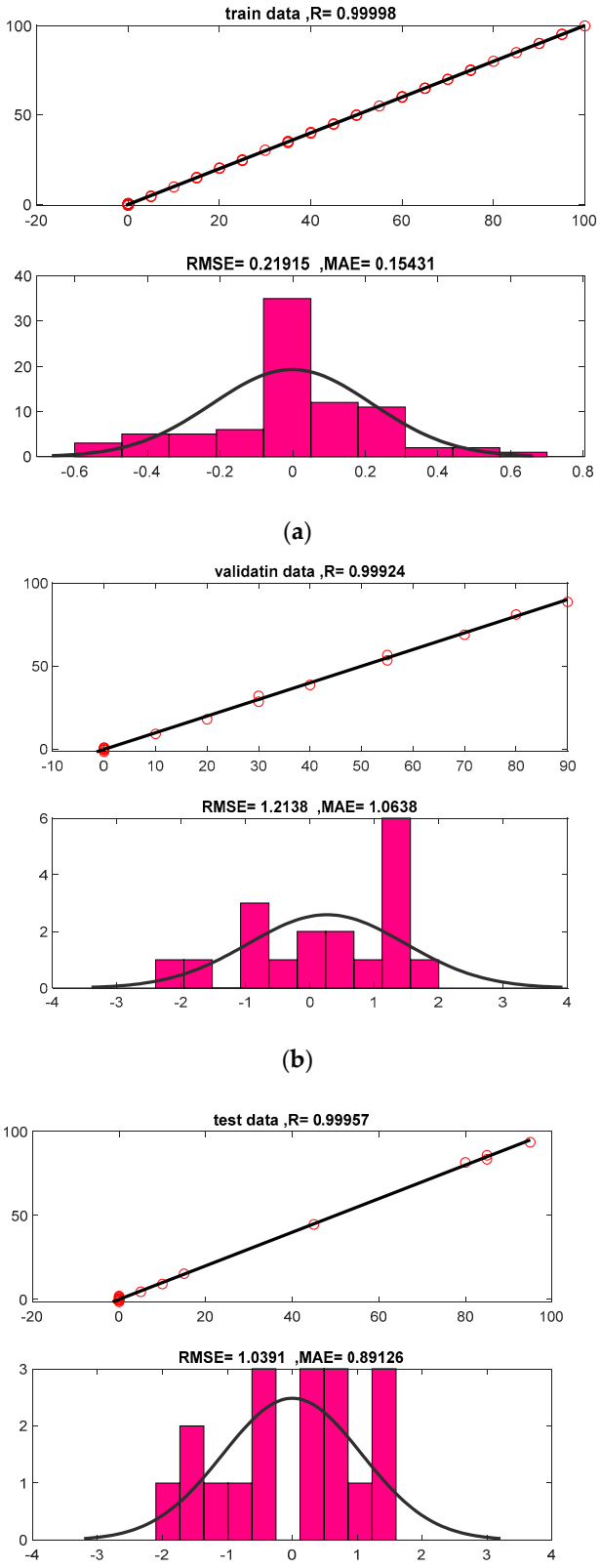

Figure 8. Operation of the designed neural network to detect the volumetric ratio of gasoil (**a**) train data, (**b**) validation data, and (**c**) test data.

The amount of these calculated errors for all three implemented networks and for training, validation and test data is shown in Table 2. The volume ratio of three products, namely ethylene glycol, crude oil, and gasoil, were obtained using an artificial neural network. The volume percentage of the fourth product (gasoline) can be easily calculated by subtracting the volume percentage of the three products from 100% of the pipe volume, which is shown graphically in Figure 9. The general process of the article to determine the percentage of volume ratios can be seen in Figure 10. The steps of determining the volume ratio include data acquisition, extracting time-domain features, introducing the most appropriate characteristics using correlation analysis, using selected features as neural network input for training, and finally, volume ratio prediction.

Table 2. The estimated error for established networks.

	Train Data		Validation Data		Test Data	
	RMSE	**MAE**	**RMSE**	**MAE**	**RMSE**	**MAE**
Ethylene glycol	0.91	0.68	1.16	1.03	1.13	0.99
Crude oil	0.27	0.14	0.94	0.76	1.07	0.86
Gasoil	0.21	0.15	1.21	1.06	1.03	0.89

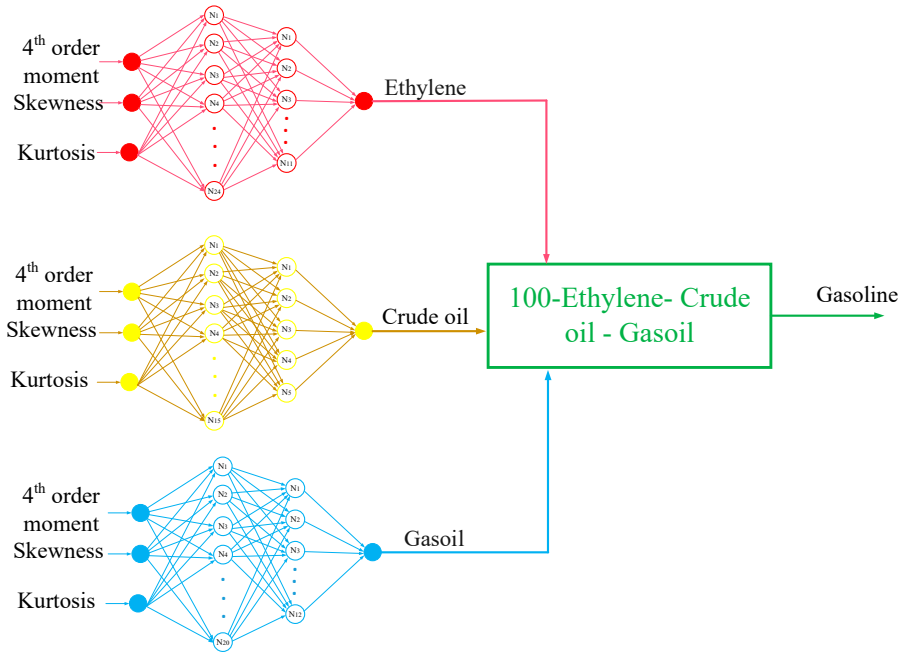

Figure 9. The general process of recognizing the volume ratio of every oil product.

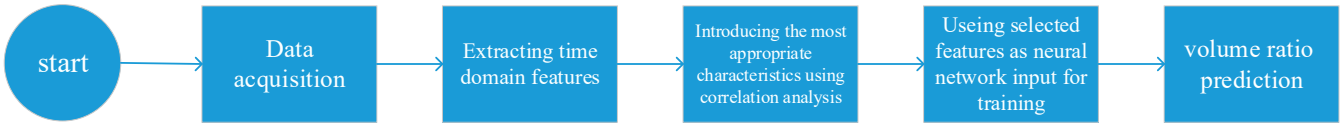

Figure 10. The process algorithm for predicting volume ratio.

6. Discussion

In this study, for designing neural networks with high accuracy, networks with a different number of layers, from one layer to four layers, and with a different number of neurons in each layer were designed and their accuracy was examined. The design of these neural networks was achieved with the help of MATLAB R2018b software, and in this software, there is a function called "newff" for designing the multilayer perceptron neural

network. No pre-designed toolboxes have been used and all the steps of training, validation, and testing of the network have been programmed step by step. The Levenberg–Marquardt algorithm has been used to train neural networks. This function does not provide users with any information about parameters such as momentum and learning rate, and the important challenge in using this function is to design a suitable structure to predict the target output with high accuracy. The high accuracy obtained in this research is a strong reason for the high performance of designed networks.

7. Conclusions

In the proposed article, the monitoring system consists of an X-ray tube, a NaI detector, and a pipe that has been simulated by MCNPX code. By simulating the combination of four petroleum products in diverse volume ratios and data collection registered by the detector, the time domain feature extraction method was utilized to derive the data characteristics, and a correlation analysis was applied to determine efficient ones. After that, the derived specifications were applied for implementing three MLP neural networks to predict the volume ratio of ethylene glycol, crude oil and gasoil. The designed networks were able to predict the volume ratio of ethylene glycol, crude oil and gasoil with RMSE less than 1.16, 1.07, and 1.21, respectively. It is highly noted that after estimating the volume ratio of three products, the volume ratio of the fourth product is feasibly estimated. Although the X-ray tube and radioisotopes have been utilized in previous research, applying the time-domain feature extraction technique and correlation analysis are the most important novelties of the proposed investigation, in which a high precision in determining the volumetric ratio (RMSE of less than 1.21) is the most profound result of applying this method. The use of frequency and time-frequency characteristics, as well as the use of different neural networks such as GMDH and RBF, can be a good clue for researchers in future research.

Author Contributions: Conceptualization, S.M.A.; methodology, A.M.M. and K.S.N.; software, A.M.M.; investigation, K.S.N.; data curation, E.N.; writing—original draft preparation, I.M.N.; writing—review and editing, R.H.; visualization, R.H.; supervision, E.N.; funding acquisition, R.H. and I.M.N. All authors have read and agreed to the published version of the manuscript.

Funding: The authors are thankful to the Institute of Research and Consulting Studies at King Khalid University of supporting this research through grant number RGP. 2/134/42. This paper has been supported by the RUDN University Strategic Academic Leadership Program. This work is also partially supported by the Minister of Education and Science of the Republic of Poland within the "Regional Initiative of Excellence" program for years 2019–2022, project number 027/RID/2018/19.

Institutional Review Board Statement: Not applicable.

Informed Consent Statement: Not applicable.

Data Availability Statement: Not applicable.

Conflicts of Interest: The authors declare no conflict of interest.

References

1. Salgado, C.M.; Brandão, L.E.B.; Conti, C.C.; Salgado, W.L. Density prediction for petroleum and derivatives by gamma-ray attenuation and artificial neural networks. *Appl. Radiat. Isot.* **2016**, *116*, 143–149. [CrossRef] [PubMed]
2. Salgado, W.L.; Dam, R.S.; Barbosa, C.M.; da Silva, A.X.; Salgado, C.M. Monitoring system of oil by-products interface in pipelines using the gamma radiation attenuation. *Appl. Radiat. Isot.* **2020**, *160*, 109125. [CrossRef] [PubMed]
3. Åbro, E.; Johansen, G.A. Improved void fraction determination by means of multibeam gamma-ray attenuation measurements. *Flow Meas. Instrum.* **1999**, *10*, 99–108. [CrossRef]
4. Nazemi, E.; Feghhi, S.A.H.; Roshani, G.H.; Peyvandi, R.G.; Setayeshi, S. Precise Void Fraction Measurement in Two-phase Flows Independent of the Flow Regime Using Gamma-ray Attenuation. *Nucl. Eng. Technol.* **2016**, *48*, 64–71. [CrossRef]
5. Roshani, G.; Nazemi, E.; Feghhi, S. Investigation of using 60 Co source and one detector for determining the flow regime and void fraction in gas–liquid two-phase flows. *Flow Meas. Instrum.* **2016**, *50*, 73–79. [CrossRef]
6. Chunguo, J.; Qiuguo, B. Flow regime identification of gas/liquid two-phase flow in vertical pipe using RBF neural networks. In Proceedings of the 2009 Chinese Control and Decision Conference, Guilin, China, 17–19 June 2009; pp. 5143–5147. [CrossRef]

7. Peyvandi, R.G.; Rad, S.Z.I. Application of artificial neural networks for the prediction of volume fraction using spectra of gamma rays backscattered by three-phase flows. *Eur. Phys. J. Plus* **2017**, *132*, 511. [CrossRef]
8. Roshani, G.H.; Nazemi, E.; Roshani, M.M. Intelligent recognition of gas-oil-water three-phase flow regime and deter-mination of volume fraction using radial basis function. *Flow Meas. Instrum.* **2017**, *54*, 39–45. [CrossRef]
9. Roshani, G.; Nazemi, E.; Roshani, M. Identification of flow regime and estimation of volume fraction independent of liquid phase density in gas-liquid two-phase flow. *Prog. Nucl. Energy* **2017**, *98*, 29–37. [CrossRef]
10. Roshani, G.H.; Nazemi, E.; Feghhi, S.A.; Setayeshi, S. Flow regime identification and void fraction prediction in two-phase flows based on gamma ray attenuation. *Measurment* **2015**, *62*, 25–32. [CrossRef]
11. Nazemi, E.; Roshani, G.H.; Feghhi, S.A.H.; Setayeshi, S.; Zadeh, E.E.; Fatehi, A. Optimization of a method for identifying the flow regime and measuring void fraction in a broad beam gamma-ray attenuation technique. *Int. J. Hydrogen Energy* **2016**, *41*, 7438–7444. [CrossRef]
12. Roshani, G.H.; Nazemi, E.; Shama, F.; Imani, M.A.; Mohammadi, S. Designing a simple ra-diometric system to predict void fraction percentage independent of flow pattern using radial basis function. *Metrol. Meas. Syst.* **2018**, *25*, 347–358.
13. Roshani, G.H.; Karami, A.; Nazemi, E.; Shama, F. Volume fraction determination of the annular three-phase flow of gas-oil-water using adaptive neuro-fuzzy inference system. *Comput. Appl. Math.* **2018**, *37*, 4321–4341. [CrossRef]
14. Roshani, G.; Karami, A.; Khazaei, A.; Olfateh, A.; Nazemi, E.; Omidi, M. Optimization of radioactive sources to achieve the highest precision in three-phase flow meters using Jaya algorithm. *Appl. Radiat. Isot.* **2018**, *139*, 256–265. [CrossRef]
15. Roshani, M.; Sattari, M.A.; Ali, P.J.M.; Roshani, G.H.; Nazemi, B.; Corniani, E.; Nazemi, E. Application of GMDH neural network technique to improve measuring precision of a simplified photon attenuation based two-phase flowmeter. *Flow Meas. Instrum.* **2020**, *75*, 101804. [CrossRef]
16. Hanus, R.; Zych, M.; Petryka, L.; Jaszczur, M.; Hanus, P. Signals features extraction in liquid-gas flow measurements using gamma densitometry. Part 1: Time domain. *EPJ Web Conf.* **2016**, *114*, 02035. [CrossRef]
17. Sattari, M.A.; Roshani, G.H.; Hanus, R.; Nazemi, E. Applicability of time-domain fea-ture extraction methods and artificial intelligence in two-phase flow meters based on gamma-ray absorption technique. *Measurement* **2021**, *168*, 108474. [CrossRef]
18. Cocchi, L.; Passaro, S.; Caratori Tontini, F.; Ventura, G. Volcanism in slab tear faults is larger than in island-arcs and back-arcs. *Nat. Commun.* **2017**, *8*, 1451. [CrossRef]
19. Hosseini, S.; Roshani, G.; Setayeshi, S. Precise gamma based two-phase flow meter using frequency feature extraction and only one detector. *Flow Meas. Instrum.* **2020**, *72*, 101693. [CrossRef]
20. Sattari, M.A.; Roshani, G.H.; Hanus, R. Improving the structure of two-phase flow meter using feature extraction and GMDH neural network. *Radiat. Phys. Chem.* **2020**, *171*, 108725. [CrossRef]
21. Roshani, G.H.; Ali, P.J.M.; Mohammed, S.; Hanus, R.; Abdulkareem, L.; Alanezi, A.A.; Sattari, M.A.; Amiri, S.; Nazemi, E.; Eftekhari-Zadeh, E.; et al. Simulation Study of Utilizing X-ray Tube in Monitoring Systems of Liquid Petroleum Products. *Processes* **2021**, *9*, 828. [CrossRef]
22. Basahel, A.; Sattari, M.; Taylan, O.; Nazemi, E. Application of Feature Extraction and Artificial Intelligence Techniques for Increasing the Accuracy of X-ray Radiation Based Two Phase Flow Meter. *Mathematics* **2021**, *9*, 1227. [CrossRef]
23. Alamoudi, M.; Sattari, M.; Balubaid, M.; Eftekhari-Zadeh, E.; Nazemi, E.; Taylan, O.; Kalmoun, E. Application of Gamma Attenuation Technique and Artificial Intelligence to Detect Scale Thickness in Pipelines in Which Two-Phase Flows with Different Flow Regimes and Void Fractions Exist. *Symmetry* **2021**, *13*, 1198. [CrossRef]
24. Taylan, O.; Sattari, M.A.; Essoussi, I.E.; Nazemi, E. Frequency Domain Feature Extraction Investigation to Increase the Accuracy of an Intelligent Nondestructive System for Volume Fraction and Regime Determination of Gas-Water-Oil Three-Phase Flows. *Mathematics* **2021**, *9*, 2091. [CrossRef]
25. Roshani, M.; Phan, G.; Roshani, G.H.; Hanus, R.; Nazemi, B.; Corniani, E.; Nazemi, E. Combination of X-ray tube and GMDH neural network as a nondestructive and potential technique for measuring characteristics of gas-oil–water three phase flows. *Measurement* **2021**, *168*, 108427. [CrossRef]
26. Meric, I.; Johansen, G.A.; Mattingly, J.; Gardner, R. On the ill-conditioning of the multiphase flow measurement by prompt gamma-ray neutron activation analysis. *Radiat. Phys. Chem.* **2014**, *95*, 401–404. [CrossRef]
27. Holstad, M.B.; A Johansen, G. Produced water characterization by dual modality gamma-ray measurements. *Meas. Sci. Technol.* **2005**, *16*, 1007–1013. [CrossRef]
28. Pelowitz, D.B. *MCNP-X TM User's Manual, Version 2.5.0. LA-CP-05e0369*; Los Alamos National Laboratory: Los Alamos, NM, USA, 2005.
29. Hernandez, A.M.; Boone, J.M. Tungsten anode spectral model using interpolating cubic splines: Unfiltered X-ray spectra from 20 kV to 640 kV. *Med. Phys.* **2014**, *41*, 042101. [CrossRef]
30. Rodriguez-Ibarra, J.L.; Hernandez-Adame, P.L.; Vega-Carrillo, H.R.; Rivera, T. X-ray spectra and doses. *Appl. Radiat. Isot.* **2016**, *117*, 32–35. [CrossRef]
31. Poludniowski, G.; Landry, G.; Deblois, F.; Evans, P.M.; Verhaegen, F. SpekCalc: A program to calculate photon spectra from tungsten anode X-ray tubes. *Phys. Med. Biol.* **2009**, *54*, N433. [CrossRef]
32. Aleksandrov, A.N. Simulating the formation of wax deposits in wells using electric submersible pumps. In *Advances in Raw Material Industries for Sustainable Development Goals*; CRC Press: London, UK, 2021; pp. 283–295.

33. Wang, Q.; Zhao, X.; Zhang, J.; Zhang, P.; Wang, X.; Yang, C.; Wang, J.; Wu, Z. Research on Quality Characterization Method of Micro-Injection Products Based on Cavity Pressure. *Polymers* **2021**, *13*, 2755. [CrossRef]
34. Roth, B.; Drummer, D. Pressure Equilibrium Time of a Cyclic-Olefin Copolymer. *Polymers* **2021**, *13*, 2309. [CrossRef] [PubMed]
35. Khounani, Z.; Hosseinzadeh-Bandbafha, H.; Nazemi, F.; Shaeifi, M.; Karimi, K.; Tabatabaei, M.; Aghbashlo, M.; Lam, S.S. Exergy analysis of a whole-crop safflower biorefinery: A step towards reducing agricultural wastes in a sustainable manner. *J. Environ. Manag.* **2020**, *279*, 111822. [CrossRef] [PubMed]
36. Karpikov, A.V.; I Aliev, R.; Babyr, N.V. An analysis of the effectiveness of hydraulic fracturing at YS1 of the Northern field. *IOP Conf. Ser. Mater. Sci. Eng.* **2020**, *952*, 012036. [CrossRef]
37. Prischepa, O.M.; Nefedov, Y.V.; Kochneva, O.E. Raw material base of hard-to-extract oil reserves of Russia. Matéria-prima base de reservas de óleo de difícil extração da Rússia. *Period. Tche Quim.* **2020**, *17*, 915–924.
38. Choi, J.; Kim, Y. A Heterogeneous Learning Framework for Over-the-Top Consumer Analysis Reflecting the Actual Market Environment. *Appl. Sci.* **2021**, *11*, 4783. [CrossRef]
39. Rožanec, J.; Kažič, B.; Škrjanc, M.; Fortuna, B.; Mladenić, D. Automotive OEM Demand Forecasting: A Comparative Study of Forecasting Algorithms and Strategies. *Appl. Sci.* **2021**, *11*, 6787. [CrossRef]
40. Villaseñor, C.; Gallegos, A.A.; Lopez-Gonzalez, G.; Gomez-Avila, J.; Hernandez-Barragan, J.; Arana-Daniel, N. Ellipsoidal Path Planning for Unmanned Aerial Vehicles. *Appl. Sci.* **2021**, *11*, 7997. [CrossRef]
41. Alhammad, N.; Al-Dossari, H. Dynamic Segmentation for Physical Activity Recognition Using a Single Wearable Sensor. *Appl. Sci.* **2021**, *11*, 2633. [CrossRef]
42. Moradi, M.J.; Hariri-Ardebili, M.A. Developing a Library of Shear Walls Database and the Neural Network Based Predictive Meta-Model. *Appl. Sci.* **2019**, *9*, 2562. [CrossRef]
43. Nazemi, B.; Rafiean, M. Forecasting house prices in Iran using GMDH. *Int. J. Hous. Mark. Anal.* **2020**, *14*, 555–568. [CrossRef]
44. Nazemi, B.; Rafiean, M. Modelling the affecting factors of housing price using GMDH-type artificial neural networks in Isfahan city of Iran. *Int. J. Hous. Mark. Anal.* **2021**, *15*. [CrossRef]
45. Karami, A.; Roshani, G.H.; Khazaei, A.; Nazemi, E.; Fallahi, M. Investigation of different sources in order to optimize the nuclear metering system of gas–oil–water annular flows. *Neural Comput. Appl.* **2018**, *32*, 3619–3631. [CrossRef]
46. Alanazi, A.K.; Alizadeh, S.M.; Nurgalieva, K.S.; Guerrero, J.W.G.; Abo-Dief, H.M.; Eftekhari-Zadeh, E.; Nazemi, E.; Narozhnyy, I.M. Optimization of X-ray Tube Voltage to Improve the Precision of Two Phase Flow Meters Used in Petroleum Industry. *Sustainability* **2021**, *13*, 13622. [CrossRef]
47. Golijanek-Jędrzejczyk, A.; Mrowiec, A.; Hanus, R.; Zych, M.; Heronimczak, M.; Świsulski, D. The assessment of metrological properties of segmental orifice based on simulations and experiments. *Measurement* **2021**, *181*, 109601. [CrossRef]
48. Alanazi, A.K.; Alizadeh, S.M.; Nurgalieva, K.S.; Nesic, S.; Grimaldo Guerrero, J.W.; Abo-Dief, H.M.; Eftekhari-Zadeh, E.; Nazemi, E.; Narozhnyy, I.M. Application of Neural Network and Time-Domain Feature Extraction Techniques for Determining Volumetric Percentages and the Type of Two Phase Flow Regimes Independent of Scale Layer Thickness. *Appl. Sci.* **2022**, *12*, 1336. [CrossRef]
49. Zych, M.; Petryka, L.; Kępiński, J.; Hanus, R.; Bujak, T.; Puskarczyk, E. Radioisotope investigations of compound two-phase flows in an open channel. *Flow Meas. Instrum.* **2014**, *35*, 11–15. [CrossRef]
50. Roshani, M.; Phan, G.T.; Ali, P.J.M.; Roshani, G.H.; Hanus, R.; Duong, T.; Corniani, E.; Nazemi, E.; Kalmoun, E.M. Evalua-tion of flow pattern recognition and void fraction measurement in two phase flow independent of oil pipeline's scale layer thickness. *Alex. Eng. J.* **2021**, *60*, 1955–1966. [CrossRef]
51. Nguyen, V.T.; Rogachev, M.K.; Aleksandrov, A.N. A new approach to improving efficiency of gas-lift wells in the conditions of the formation of organic wax deposits in the Dragon field. *J. Pet. Explor. Prod. Technol.* **2020**, *10*, 3663–3672. [CrossRef]
52. Dolgii, I.E. Methods to enhance oil recovery in the process of complex field development of the Yarega oil and titanium deposit. *J. Min. Inst.* **2017**, *231*, 263–297.
53. Gabdrakhmanov, N.K.; Mingulov, S.G.; Strizhnev, V.A.; Karimov, R.D. Diagnostics of field pipelines as a means of improving the reliability of pipeline systems. *J. Min. Inst.* **2005**, *164*, 5.
54. Sandyga, M.S.; Struchkov, I.A.; Rogachev, M.K. Formation damage induced by wax deposition: Laboratory investigations and modeling. *J. Pet. Explor. Prod. Technol.* **2020**, *10*, 2541–2558. [CrossRef]
55. Sultanbekov, R. Research of the influence of marine residual fuel composition on sedimentation due to incompatibility. *J. Mar. Sci. Eng.* **2021**, *9*, 1067. [CrossRef]
56. Kashnikov, Y.A.; Ashikhmin, S.; Kukhtinskii, A.; Shustov, D.V. The relationship of fracture toughness coefficients and geophysical characteristics of rocks of hydrocarbon deposits. *J. Min. Inst.* **2020**, *241*, 83. [CrossRef]
57. Belonogov, E.V.; Korovin, A.Y.; Yakovlev, A.A. Increase of the injectivity coefficient by dynamic development of injection wells. *J. Min. Inst.* **2019**, *1*, 238.
58. Grigorev, B.M.; Tananykhin, D.; Poroshin, A.M. Sand management approach for a field with high viscosity oil. *J. Appl. Eng. Sci.* **2020**, *18*, 64–69. [CrossRef]
59. Shagiakhmetov, A.M.; Podoprigora, D.G.; Terleev, A.V. The study of the dependence of the rheological properties of gel-forming compositions on the crack opening when modeling their flow on a rotational viscometer. *Period. Tche Quim.* **2020**, *17*, 933–939.
60. Galkin, S.V.; Kochnev, A.A.; Zotikov, V.I. Predictive assessment of the effectiveness of radial drilling technology for the Bashkir production facilities of the Perm Territory fields. *J. Min. Inst.* **2019**, *1*, 238.

61. Molchanov, A.A.; Ageev, P.G. Implementation of new technologies is a reliable way of extracting residual reserves of hydro-carbon deposits. *J. Min. Inst.* **2017**, *1*, 227.
62. Morenov, V.; Leusheva, E.; Martel, A. Investigation of the Fractional Composition Effect of the Carbonate Weighting Agents on the Rheology of the Clayless Drilling Mud. *Int. J. Eng.* **2018**, *31*. [CrossRef]
63. Nikitin, M.; Saychenko, L. The rheological properties of abnormally viscous oil. *Pet. Sci. Technol.* **2017**, *36*, 136–140. [CrossRef]
64. Ruiz-Morales, B.; Espitia-Moreno, I.; Alfaro-Garcia, V.; Leon-Castro, E. Sustainable Development Goals Analysis with Ordered Weighted Average Operators. *Sustainability* **2021**, *13*, 5240. [CrossRef]
65. Francik, S.; Knapczyk, A.; Knapczyk, A.; Francik, R. Decision Support System for the Production of Miscanthus and Willow Briquettes. *Energies* **2020**, *13*, 1364. [CrossRef]
66. Taylor, J.G. *Neural Networks and Their Applications*; John Wiley & Sons Ltd.: Brighton, UK, 1996.
67. Gallant, A.R.; White, H. On learning the derivatives of an unknown mapping with multilayer feedforward networks. *Neural Netw.* **1992**, *5*, 129–138. [CrossRef]
68. Song, Y.-Q.; Zhao, T.-H.; Chu, Y.-M.; Zhang, X.-H. Optimal evaluation of a Toader-type mean by power mean. *J. Inequal. Appl.* **2015**, *2015*, 408. [CrossRef]
69. Hu, S.; Wu, H.; Liang, X.; Xiao, C.; Zhao, Q.; Cao, Y.; Han, X. A preliminary study on the eco-environmental geological issue of in-situ oil shale mining by a physical model. *Chemosphere* **2021**, *287*, 131987. [CrossRef]
70. Chu, Y.; Zhao, T.-H. Concavity of the error function with respect to Hölder means. *Math. Inequal. Appl.* **1998**, 589–595. [CrossRef]
71. Shen, Z.; Wang, F.; Wang, Z.; Li, J. A critical review of plant-based insulating fluids for transformer: 30-year development. *Renew. Sustain. Energy Rev.* **2021**, *141*, 110783. [CrossRef]
72. Zhao, T.-H.; He, Z.-Y.; Chu, Y.-M. On some refinements for inequalities involving zero-balanced hypergeometric function. *AIMS Math.* **2020**, *5*, 6479–6495. [CrossRef]
73. Cheng, H.; Sun, L.; Wang, Y.; Chen, X. Effects of actual loading waveforms on the fatigue behaviours of asphalt mixtures. *Int. J. Fatigue* **2021**, *151*, 106386. [CrossRef]
74. Zhao, T.-H.; Wang, M.-K.; Chu, Y.-M. A sharp double inequality involving generalized complete elliptic integral of the first kind. *AIMS Math.* **2020**, *5*, 4512–4528. [CrossRef]
75. Sun, J.; Wang, Y.; Liu, S.; Dehghani, A.; Xiang, X.; Wei, J.; Wang, X. Mechanical, chemical and hydrothermal activation for waste glass reinforced cement. *Constr. Build. Mater.* **2021**, *301*, 124361. [CrossRef]
76. Jin, F.; Qian, Z.-S.; Chu, Y.-M.; Rahman, M.U. On nonlinear evolution model for drinking behavior under caputo-fabrizio derivative. *J. Appl. Anal. Comput.* **2020**. [CrossRef]
77. Iqbal, A.; Wang, Y.; Miah, M.; Osman, M.S. Study on Date–Jimbo–Kashiwara–Miwa Equation with Conformable Derivative Dependent on Time Parameter to Find the Exact Dynamic Wave Solutions. *Fractal Fract.* **2021**, *6*, 4. [CrossRef]
78. Zhao, T.-H.; He, Z.-Y.; Chu, Y.-M. Sharp Bounds for the Weighted Hölder Mean of the Zero-Balanced Generalized Complete Elliptic Integrals. *Comput. Methods Funct. Theory* **2020**, *21*, 413–426. [CrossRef]
79. He, Z.-Y.; Abbes, A.; Jahanshahi, H.; Alotaibi, N.D.; Wang, Y. Fractional-Order Discrete-Time SIR Epidemic Model with Vaccination: Chaos and Complexity. *Mathematics* **2022**, *10*, 165. [CrossRef]
80. Chu, H.-H.; Zhao, T.-H.; Chu, Y.-M. Sharp bounds for the Toader mean of order 3 in terms of arithmetic, quadratic and contraharmonic means. *Math. Slovaca* **2020**, *70*, 1097–1112. [CrossRef]
81. Zhao, T.-H.; Wang, M.-K.; Chu, Y. Concavity and bounds involving generalized elliptic integral of the first kind. *J. Math. Inequal.* **2007**, 701–724. [CrossRef]
82. Chu, Y.-M.; Zhao, T.-H. Convexity and concavity of the complete elliptic integrals with respect to Lehmer mean. *J. Inequal. Appl.* **2015**, *2015*, 396. [CrossRef]
83. Chu, Y.-M.; Wang, H.; Zhao, T.-H. Sharp bounds for the Neuman mean in terms of the quadratic and second Seiffert means. *J. Inequal. Appl.* **2014**, *2014*, 299. [CrossRef]
84. Sun, H.; Zhao, T.-H.; Chu, Y.; Liu, B. A note on the Neuman-Sándor mean. *J. Math. Inequal.* **2007**, *8*, 287–297. [CrossRef]
85. Wang, M.-K.; Hong, M.-Y.; Xu, Y.-F.; Shen, Z.-H.; Chu, Y. Inequalities for generalized trigonometric and hyperbolic functions with one parameter. *J. Math. Inequal.* **2007**, *14*, 1–21. [CrossRef]
86. Karthikeyan, K.; Karthikeyan, P.; Baskonus, H.M.; Venkatachalam, K.; Chu, Y. Almost sectorial operators on Ψ-Hilfer derivative fractional impulsive integro-differential equations. *Math. Methods Appl. Sci.* **2021**. [CrossRef]
87. Lalbakhsh, A.; Mohamadpour, G.; Roshani, S.; Ami, M.; Roshani, S.; Sayem, A.S.M.; Alibakhshikenari, M.; Koziel, S. Design of a Compact Planar Transmission Line for Miniaturized Rat-Race Coupler with Harmonics Suppression. *IEEE Access* **2021**, *9*, 129207–129217. [CrossRef]
88. Roshani, S.; Koziel, S.; Roshani, S.; Jamshidi, M.B.; Parandin, F.; Szczepanski, S. Design of a Patch Power Divider with Simple Structure and Ultra-Broadband Harmonics Suppression. *IEEE Access* **2021**, *9*, 165734–165744. [CrossRef]
89. Pirasteh, A.; Roshani, S.; Roshani, S. A modified class-F power amplifier with miniaturized harmonic control circuit. *AEU Int. J. Electron. Commun.* **2018**, *97*, 202–209. [CrossRef]
90. Roshani, S.; Roshani, S.; Zarinitabar, A. A modified Wilkinson power divider with ultra harmonic suppression using open stubs and lowpass filters. *Analog Integr. Circuits Signal Process.* **2018**, *98*, 395–399. [CrossRef]
91. Roshani, S.; Roshani, S. Design of a very compact and sharp bandpass diplexer with bended lines for GSM and LTE applications. *AEU Int. J. Electron. Commun.* **2018**, *99*, 354–360. [CrossRef]

92. Pirasteh, A.; Roshani, S.; Roshani, S. Compact microstrip lowpass filter with ultrasharp response using a square-loaded modified T-shaped resonator. *Turk. J. Electr. Eng. Comput. Sci.* **2018**, *26*, 1736–1746. [CrossRef]
93. Roshani, S.; Roshani, S. Design of a compact LPF and a miniaturized Wilkinson power divider using aperiodic stubs with harmonic suppression for wireless applications. *Wirel. Netw.* **2019**, *26*, 1493–1501. [CrossRef]
94. Heshmati, H.; Roshani, S. A miniaturized lowpass bandpass diplexer with high isolation. *AEU Int. J. Electron. Commun.* **2018**, *87*, 87–94. [CrossRef]
95. Roshani, S. A compact microstrip low-pass filter with ultra wide stopband using compact microstrip resonant cells. *Int. J. Microw. Wirel. Technol.* **2016**, *9*, 1023–1027. [CrossRef]
96. Jamshidi, M.; Siahkamari, H.; Roshani, S.; Roshani, S. A compact Gysel power divider design using U-shaped and T-shaped resonators with harmonics suppression. *Electromagnetics* **2019**, *39*, 491–504. [CrossRef]
97. Jamshidi, M.B.; Roshani, S.; Talla, J.; Roshani, S.; Peroutka, Z. Size reduction and performance improvement of a microstrip Wilkinson power divider using a hybrid design technique. *Sci. Rep.* **2021**, *11*, 7773. [CrossRef]
98. Roshani, S.; Roshani, S. Design of a high efficiency class-F power amplifier with large signal and small signal measurements. *Measurement* **2019**, *149*, 106991. [CrossRef]
99. Hookari, M.; Roshani, S.; Roshani, S. High-efficiency balanced power amplifier using miniaturized harmonics suppressed coupler. *Int. J. RF Microw. Comput. Eng.* **2020**, *30*, e22252. [CrossRef]
100. Roshani, S.; Roshani, S. Two-Section Impedance Transformer Design and Modeling for Power Amplifier Applications. *Appl. Comput. Electromagn. Soc. J.* **2017**, *32*, 1042–1047.
101. Roshani, S.; Jamshidi, M.B.; Mohebi, F.; Roshani, S. Design and Modeling of a Compact Power Divider with Squared Resonators Using Artificial Intelligence. *Wirel. Pers. Commun.* **2020**, *117*, 2085–2096. [CrossRef]
102. Roshani, S.; Roshani, S. A compact coupler design using meandered line compact microstrip resonant cell (MLCMRC) and bended lines. *Wirel. Netw.* **2020**, *27*, 677–684. [CrossRef]
103. Pourbemany, J.; Zhu, Y.; Bettati, R. Breath to Pair (B2P): Respiration-Based Pairing Protocol for Wearable Devices. *arXiv* **2021**, arXiv:2107.11677.
104. Pourbemany, J.; Zhu, Y.; Bettati, R. A Survey of Wearable Devices Pairing Based on Biometric Signals. *arXiv* **2021**, arXiv:2107.11685.
105. Seaberg, J.; Kaabipour, S.; Hemmati, S.; Ramsey, J.D. A rapid millifluidic synthesis of tunable polymer-protein nanoparticles. *Eur. J. Pharm. Biopharm.* **2020**, *154*, 127–135. [CrossRef] [PubMed]
106. Charchi, N.; Li, Y.; Huber, M.; Kwizera, E.A.; Huang, X.; Argyropoulos, C.; Hoang, T. Small mode volume plasmonic film-coupled nanostar resonators. *Nanoscale Adv.* **2020**, *2*, 2397–2403. [CrossRef] [PubMed]
107. Rezaei, T.; Aslmarand, S.M.; Snyder, R.; Khajavi, B.; Alsing, P.M.; Fanto, M.; Miller, W.A. Experimental realization of Schumacher's information geometric Bell inequality. *Phys. Lett. A* **2021**, *405*, 127444. [CrossRef]
108. Kharazmi, O.; Jahangard, S. A new family of lifetime distributions in terms of cumulative hazard rate function. *Commun. Fac. Sci. Univ. Ank. Ser. A1 Math. Stat.* **2020**, *69*, 1–22. [CrossRef]
109. Kharazmi, O.; Saadatinik, A.; Jahangard, S. Odd Hyperbolic Cosine Exponential-Exponential (OHC-EE) Distribution. *Ann. Data Sci.* **2019**, *6*, 765–785. [CrossRef]
110. Sabzi, M.; Kamarei, M.; Haghighi, T.R.; Mahe, Y. Analysis and Design of X-Band LNA Using Parallel Technique. In Proceedings of the 2020 28th Iranian Conference on Electrical Engineering (ICEE), Tabriz, Iran, 4–6 August 2020; pp. 1–5. [CrossRef]
111. Fatholahi, M.; Anvari, A.; Akbari, O.A.; Montazerifar, F.; Ghaedamini, H.; Toghraie, D.; Nouraei, S. Numerical investigation of mixed convection of nanofluid flow in oblique rectangular microchannels with nanofluid jet injection. *Eur. Phys. J. Plus* **2021**, *136*, 1–25. [CrossRef]
112. Rastegarzadeh, S.; Mahzoon, M.; Mohammadi, H. A novel modular designing for multi-ring flywheel rotor to optimize energy consumption in light metro trains. *Energy* **2020**, *206*, 118092. [CrossRef]
113. Sabzi, M.; Kamarei, M.; Razban, T.; Mahe, Y. Optimization of LNA's first stage to reduce overall noise figure in multi-stage LNAs. *AEU Int. J. Electron. Commun.* **2020**, *123*, 153300. [CrossRef]
114. Chapnevis, A.; Guvenc, I.; Bulut, E. Traffic Shifting based Resource Optimization in Aggregated IoT Communication. In Proceedings of the 2020 IEEE 45th Conference on Local Computer Networks (LCN), Sydney, NSW, Australia, 16–19 November 2020; pp. 233–243. [CrossRef]
115. Mohaghegh, M.; Valipour, A.S. Triggering Economic Growth:Trade Liberalization as the Prominent Factor in Less-developed Countries. *Bus. Econ. Res.* **2021**, *11*, 252–265. [CrossRef]
116. Gukeh, M.J.; Damoulakis, G.; Megaridis, C.M. Experimental investigation of low-profile heat pipe with wickless wettability-patterned condenser. In Proceedings of the 2021 20th IEEE Intersociety Conference on Thermal and Thermomechanical Phenomena in Electronic Systems (iTherm), San Diego, CA, USA, 1–4 June 2021; pp. 271–279.
117. Jadidi, A.; Dizadji, M.R. Node Clustering in Binary Asymmetric Stochastic Block Model with Noisy Label Attributes via SDP. In Proceedings of the 2021 International Conference on Smart Applications, Communications and Networking (SmartNets), Glasgow, UK, 22–24 September 2021; pp. 1–6. [CrossRef]
118. Azhiri, R.B.; Jadidi, A.; Bideskan, A.S.; Dizadji, M.R. Ultrasonic nanocrystalline surface modification of low strength aluminum alloy: Trade-off between surface integrity and production rate aiming at desired fatigue life. *Int. J. Adv. Manuf. Technol.* **2021**, *113*, 1237–1251. [CrossRef]

119. Khalifehei, K.; Azizyan, G.; Shafai-Bajestan, M.; Chau, K.W. Experimental Modeling and Evaluation Sediment Scouring in Riverbeds around Downstream in Flip Buckets. *Int. J. Eng.* **2020**, *33*, 1904–1916. [CrossRef]
120. Ghaedamini, H.; Amiri, M.C. Effects of temperature and surfactant concentration on the structure and morpholo-gy of calcium carbonate nanoparticles synthesized in a colloidal gas aphrons system. *J. Mol. Liq.* **2019**, *282*, 213–220. [CrossRef]
121. Chireh, M.; Naseri, M.; Ghaedamini, H. Enhanced microwave absorption performance of graphene/doped Li fer-rite nanocomposites. *Adv. Powder Technol.* **2021**, *32*, 4697–4710. [CrossRef]
122. Carrera, F.; Dentamaro, V.; Galantucci, S.; Iannacone, A.; Impedovo, D.; Pirlo, G. Combining Unsupervised Approaches for Near Real-Time Network Traffic Anomaly Detection. *Appl. Sci.* **2022**, *12*, 1759. [CrossRef]
123. Sabzi, M. Analysis and Performance Improvement in High Frequency Wide-Band LNAs. Ph.D. Thesis, Université de Nantes, Nantes, France; Université de Téhéran, Téhéran, Iran, 2021.
124. Walid, W.; Awais, M.; Ahmed, A.; Masera, G.; Martina, M. Real-time implementation of fast discriminative scale space tracking algorithm. *J. Real-Time Image Process.* **2021**, *18*, 2347–2360. [CrossRef]
125. Shiri, A. A Novel Implementation of CORDIC Algorithm Based on Dynamic Microrotation Generation. *Mapta J. Electr. Comput. Eng. MJECE* **2021**, *3*, 17–27.